Project 5: Dynamic Mode Decomposition

Zihao Wang, Sam Minkowicz, April Zhou,
Zhongsheng Sang, Avinash Karamchandani

March 5, 2020

1 Introduction

Dynamic Mode Decomposition (DMD) is data-based algorithm to uncover modes of a system's dynamics from experimental data [1]. To uncover a system's dynamic modes DMD approximates the modes of the Koopman operator a linear, time-independent operator that maps a system from time t to time $t + j$ [2]. Specifically, consider experimental data in an $M \times N$ matrix $\mathbf{X}$ with data sampled over N spatial positions and M time-points

$$\mathbf{X} = [\mathbf{x}_1\ \mathbf{x}_2\ \cdots \mathbf{x}_M] \tag{1}$$

where $\mathbf{x}_i$ are vectors of size N. Then the Koopman operator $\mathbf{A}$ is the operator such that

$$\mathbf{X}_2^M = \mathbf{A}\mathbf{X}_1^{M-1} \tag{2}$$

where

$$\mathbf{X}_1^{M-1} = [\mathbf{x}_1\ \mathbf{x}_2\ \cdots \mathbf{x}_{M-1}] \tag{3}$$

$$\mathbf{X}_2^M = [\mathbf{x}_2\ \mathbf{x}_3\ \cdots \mathbf{x}_M] \tag{4}$$

For computational efficiency and numerical stability DMD estimates the dynamic modes of the system by performing an eigendecomposition of the matrix $\tilde{\mathbf{S}}$ which is related to $\mathbf{A}$ via a similarity transformation.

To better understand DMD and its limitations, we performed DMD on data from the Nonlinear Schrodinger equation and from the vorticity field for fluid flow past a cylinder. We describe our DMD implementation in Section 2 and the datasets in Section 3. Our results are described in Section 4 and our exploration into DMD's limitations are described in Section 5. Finally, we summarize our conclusions Section 6.

2 DMD implementation

To obtain the DMD approximation given a set of data snapshots, we implement the following algorithm:

1. Given data sampled at N grid points and M time points (evenly spaced by a fixed time step Δt), construct the data matrix $\mathbf{X} \in \mathbb{R}^{M \times N}$;
2. Construct the submatrices $\mathbf{X}_1^{M-1}$ and $\mathbf{X}_2^M$, where $\mathbf{X}_1^{M-1} = [\mathbf{x}_1\ \mathbf{x}_2\ \cdots\ \mathbf{x}_{M-1}]$ and $\mathbf{X}_2^M = [\mathbf{x}_2\ \mathbf{x}_3\ \cdots\ \mathbf{x}_M]$;
3. Compute the SVD decomposition of $\mathbf{X}_1^{M-1}$:

   $$\mathbf{X}_1^{M-1} = \mathbf{U}\mathbf{\Sigma}\mathbf{V}^*,$$

   where $\mathbf{U} \in \mathbb{C}^{N \times K}, \mathbf{\Sigma} \in \mathbb{C}^{K \times K}$, and $\mathbf{V} \in \mathbb{C}^{M-1 \times K}$;
4. Compute the matrix $\tilde{\mathbf{S}} = \mathbf{U}^*\mathbf{X}_2^M\mathbf{V}\mathbf{\Sigma}^{-1}$ and obtain its eigenvalues μ_k and eigenvectors $\mathbf{y}_k$, with $k = 1, 2, \cdots, K$;

5. Project the initial state of the system onto the DMD modes using the pseudo-inverse, i.e.,

$$\mathbf{b} = \mathbf{\Psi}^{+}\mathbf{x}_1 \quad (\longleftarrow \mathbf{x}_1 = \mathbf{\Psi}\mathbf{b}),$$

where $\mathbf{\Psi} = \mathbf{U}[\mathbf{y}_1\ \mathbf{y}_2\ \cdots \mathbf{y}_K]$;

6. Compute the solution at time t using the DMD modes along with their projection to the initial condition and the time dynamics computed using the eigenvalues μ_k, i.e.,

$$\mathbf{x}_{DMD}(t) = \mathbf{\Psi}\text{diag}(\exp(\omega t))\mathbf{b},$$

where $\omega = \ln|\mu|/\Delta t$.

3 Test systems

To better understand DMD we tested it on the following two systems.

3.1 Nonlinear Schrodinger Equation

The Nonlinear Schrodinger (NLS) equation is a classical field equation given by:

$$iu_t + \frac{1}{2}u_x x + |u|^2 u = 0 \tag{5}$$

with initial condition $Nsech(x)$. We simulated this PDE equation with FFTs using MATLAB's `fft` function. We then obtained a numerical solution with a Runge-Kutta (4,5) method via MATLAB's `ode45` function. The result of the simulation of the NLS equation over the time interval $[0, 2\pi]$ with $M = 21$ time-points and $N = 512$ spatial points is shown in Figure 1.

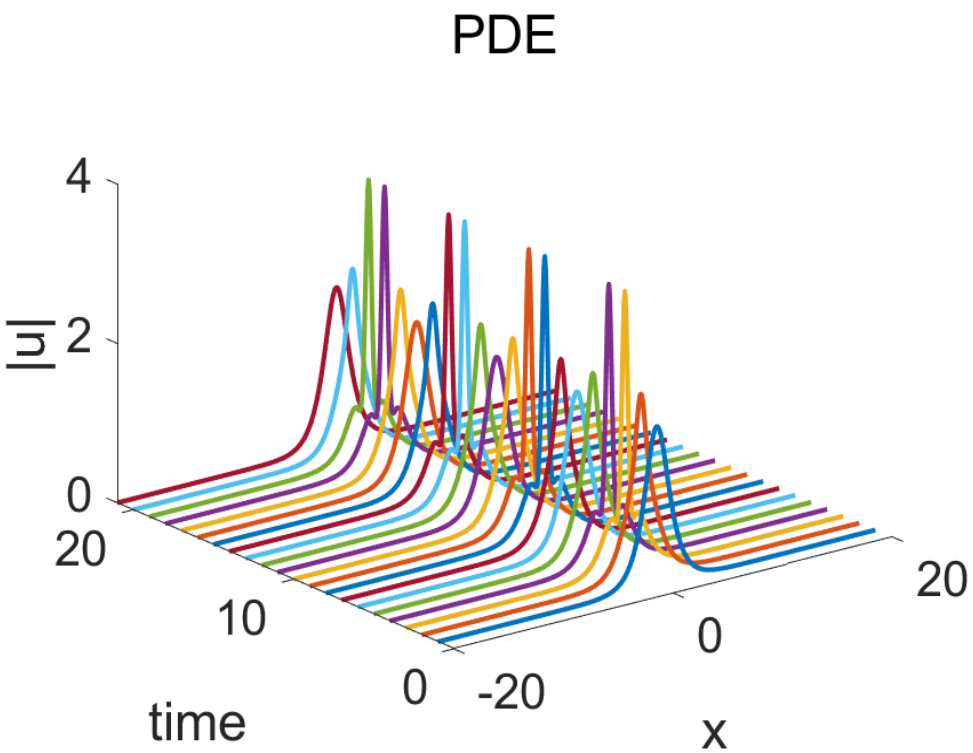

Figure 1: The numerical simulation of NLS equation over the time interval $[0, 2\pi]$ with $M = 21$ time-points and $N = 512$ spatial points

3.2 Fluid system

We were given a data set for fluid flow past a cylinder at Reynolds number 100. The data set consisted of 151 snapshots of 2-dimensional data with 199 points in the x direction and 449 points in the y direction. The data set was generated by Steven Brunton from in-compressible Naiver-Stokes equations solved by a fractional step/projection algorithm. The system is shown below in Figure 2 at snapshots 30, 60, 90, 120 and 150 from top to bottom.

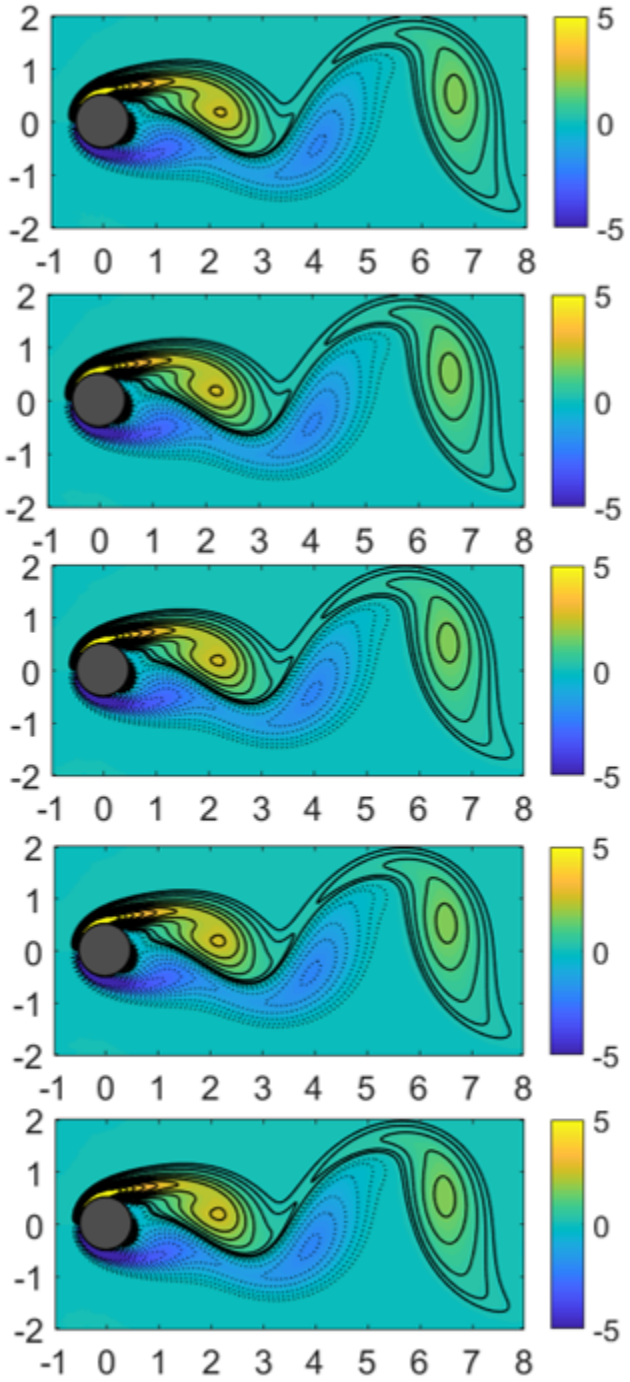

Figure 2: Simulation of fluid flow past a cylinder at Reynolds number 100 at snapshots 30, 60, 90, 120 and 150 (from top to bottom).

4 Results

4.1 Nonlinear Schrodinger equation

After solving the numerical solution of NLS equation as described in Section 3.1, we arrange the simulated data into the matrix $\mathbf{X}$ with M time points at N spatial positions. We then apply our DMD method on this matrix $\mathbf{X}$ as described in Section 2. The 20 DMD modes are shown below in Figure 3.

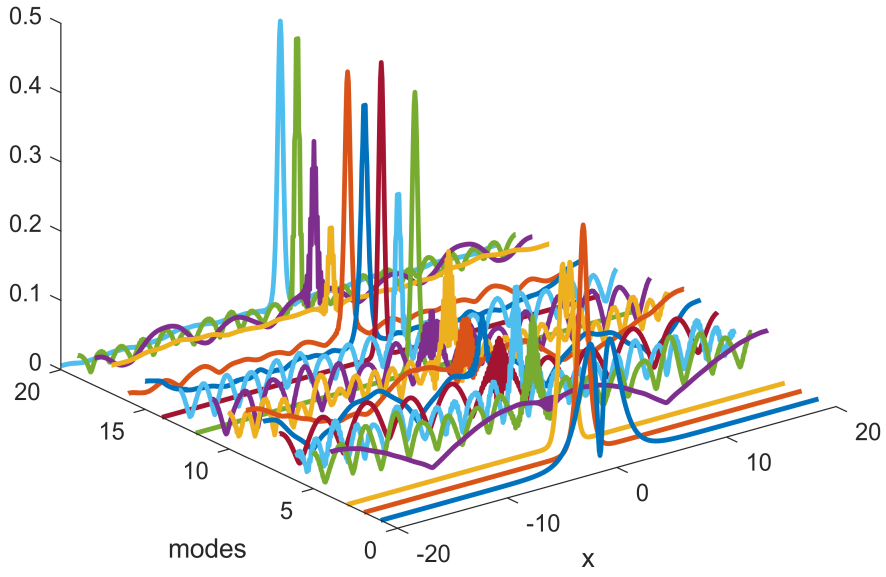

Figure 3: The DMD modes used for the linear reconstruction from the data reduction, i.e., $\psi_k = \mathbf{U}\mathbf{y}_k$, $\Psi = [\psi_1, \psi_2 ... \psi_{M-1}]$

These modes seem chaotic and oscillate rapidly. However, if we compare them with the exact solution Figure 1, we can find the large peaks are at the same position as exact solution. And the small oscillations can counteract each other, which implies these modes could predict the real solution. The PDE solution versus our DMD dynamics are shown below in Figure 4.

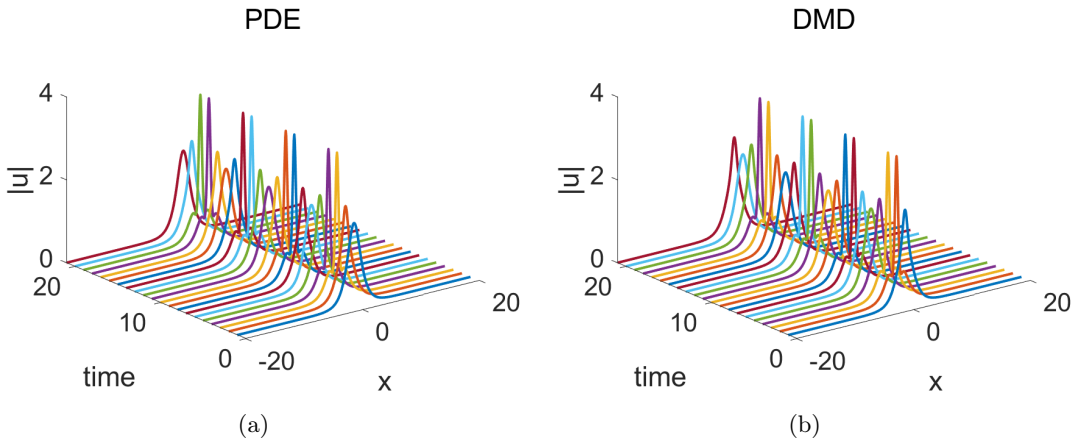

Figure 4: a) The result of the simulation of the NLS equation over the interval $[0, 2\pi]$ with $M = 21$ and $N = 512$. b) The dynamics solved by DMD method.

The DMD method seems to approximate the exact solution well for $M = 21$. The approximate solution's time evolution is determined by eigenvalues μ_k for $k = 1 : K$, which are shown below in Figure 5.

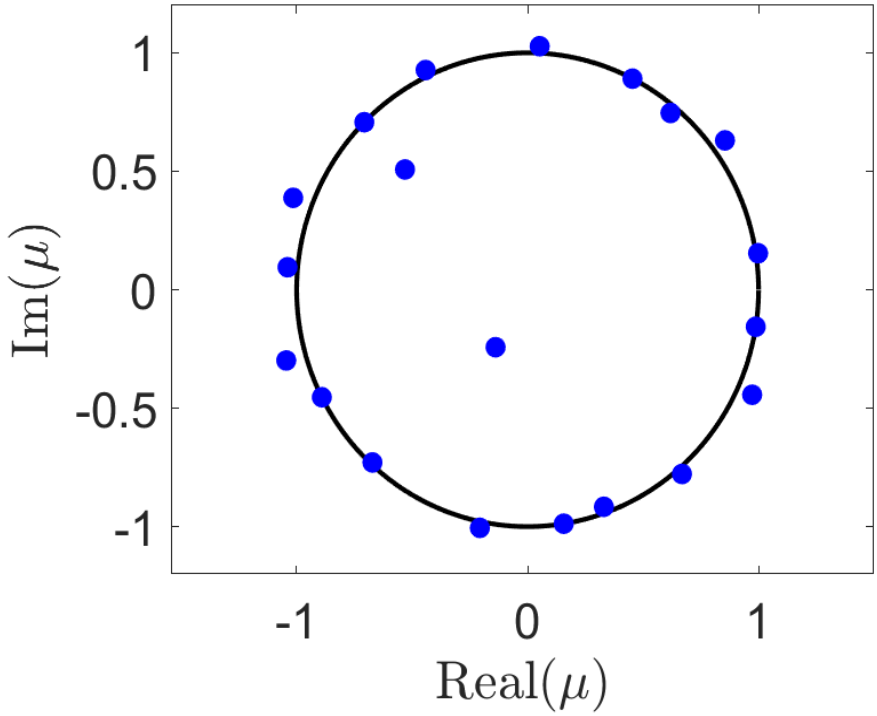

Figure 5: The eigenvalues distribution μ_k for $k = 1 : K$.

We can see the eigenvalues in blue relative to the unit circle in black. Those eigenvalues that lie outside the unit circle represent growth modes in the system. The NLS dynamics are oscillatory in time. However, our DMD method has eigenvalues out of the unit circle, which will ultimately lead to a long-term blow-up of the predicted solution. Thus, the DMD solution can only predict short-term dynamics and will fail for long term behavior.

4.2 Fluid system

We applied our DMD implementation described in Section 2 to the fluids data described in Section 3.2. Figure 6 compares the simulated data and the DMD predictions at snapshots 30, 60, 90, 120 and 150 (from top to bottom). It is clear that DMD method is successful to reconstruct the numerical simulation result of in-compressible Naiver-Stokes equation.

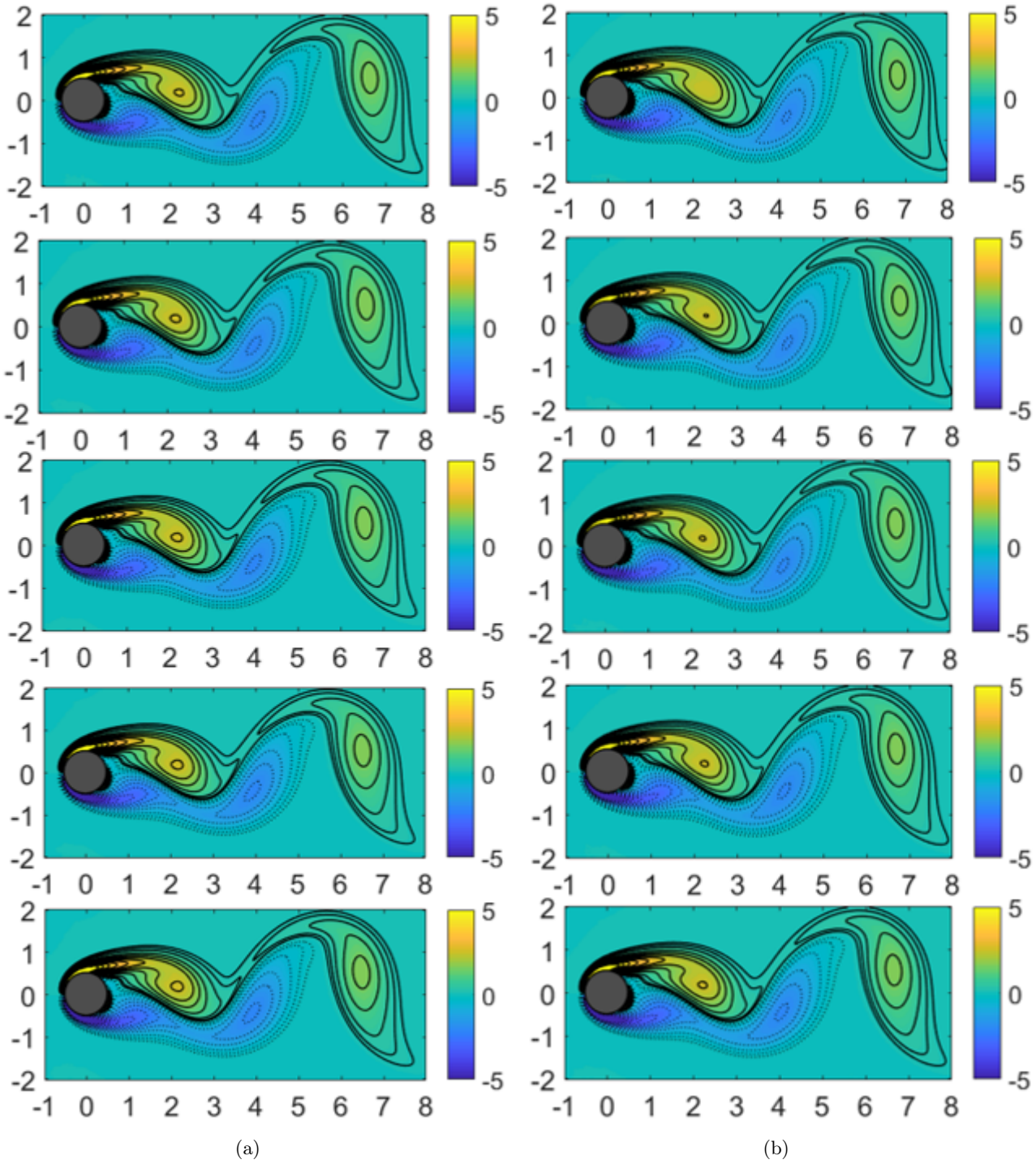

(a) (b)

Figure 6: The Comparison of (a) numerical simulation and (b) DMD result data of in-compressible Navies-Stokes equation. The snapshots from top to bottom are 30, 60, 90, 120 and 150.

12 of the DMD modes used to predict the system dynamics are shown in Figure 7. The eigenvalues are shown in Figure 8 in blue along with the unit circle in red. We can see that we don't have eigenvalues outside the unit circle thus the solution of DMD method will not blow-up. Some eigenvalues lie inside the unit circle representing the decay modes in the system. In this case, the DMD method is good at predicting the long term dynamics behavior.

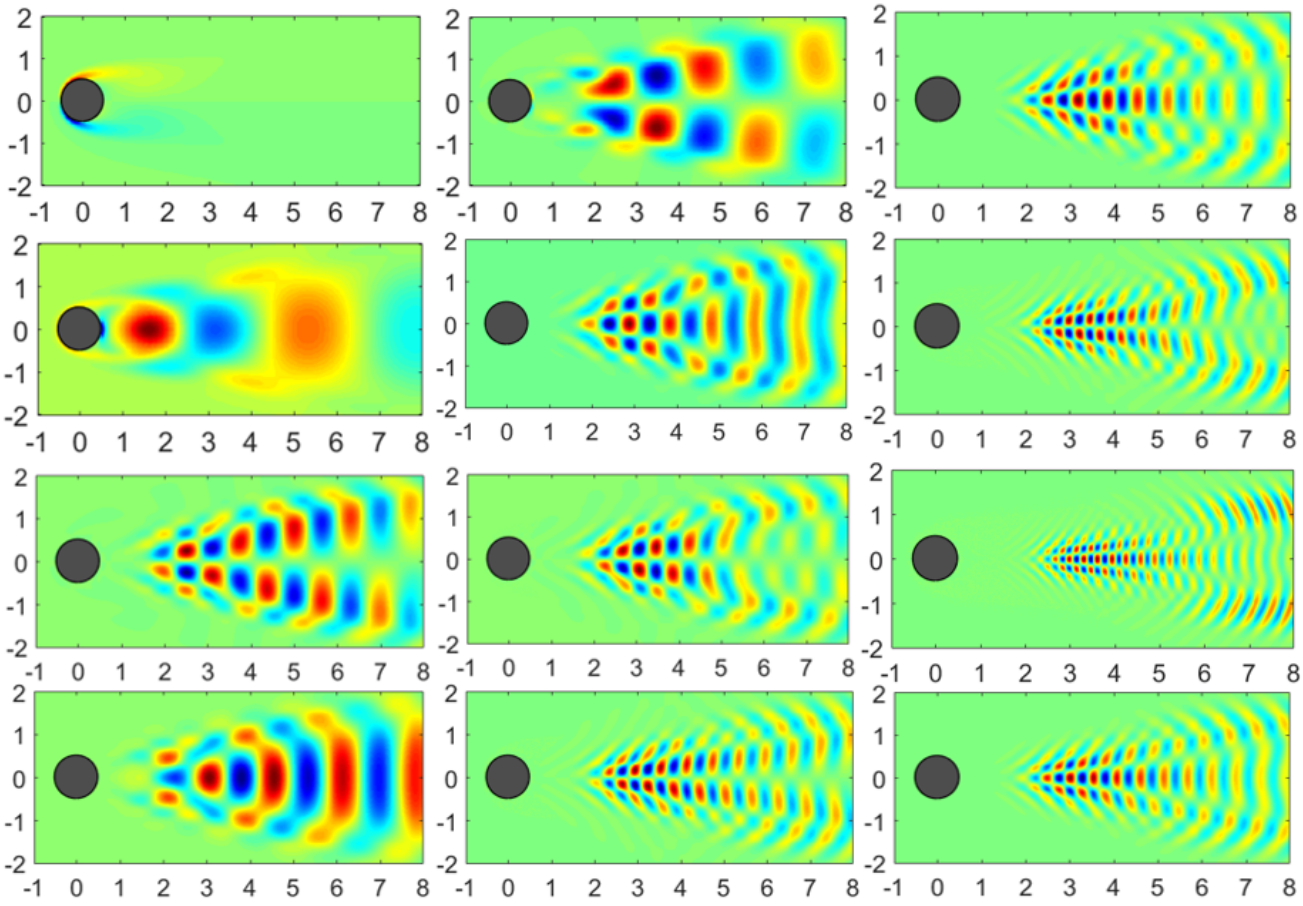

Figure 7: The DMD modes used for the linear reconstruction from the data reduction. Here are 12 most typical modes.

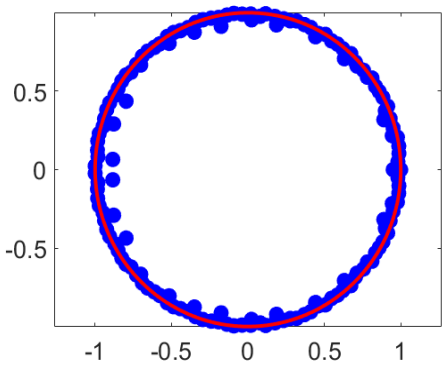

Figure 8: The eigenvalues distribution μ_k from applying DMD to the fluid data.

5 DMD limitations

To better understand DMD and its limitations we tested DMD on data from our simulation of the NLS equation with reduced sampling in time and additive measurement noise.

5.1 Reduced sampling in time

To first understand how DMD performs with reduced sampling in time we simulated the NLS equation over the time interval $[0, 2\pi]$ with $N = 512$ spatial points and $M = 15, 30, 45,$ and 60 time-points. We tested DMD on our data with each of these temporal sampling levels. Figure 9 shows the results from the simulation at each sampling level alongside the DMD prediction for the data at that sampling level. The DMD predictions seem to match the simulated data at each of these sampling levels. The DMD modes and eigenvalues at each of these sampling levels are shown in Figure 10. We can now see that as M increases the eigenvalues get closer to the unit circle and thus we can expect DMD predictions to become better for longer timescales.

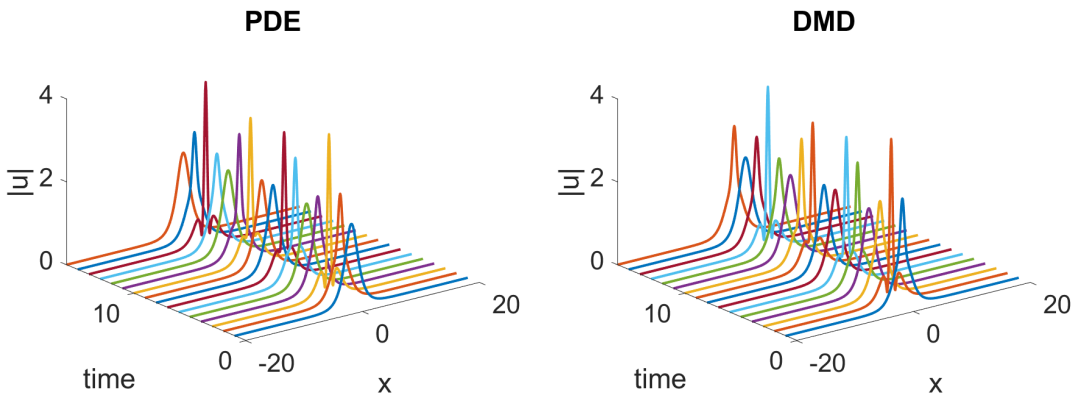

(a) (b)

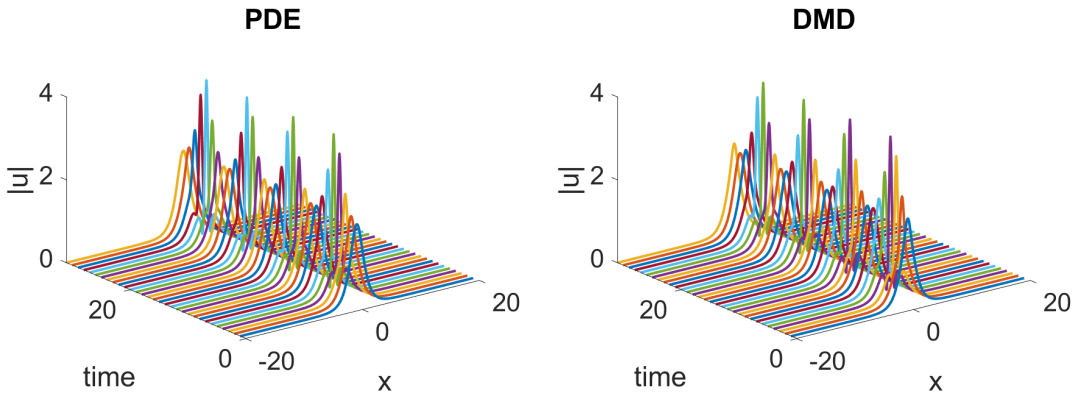

(c) (d)

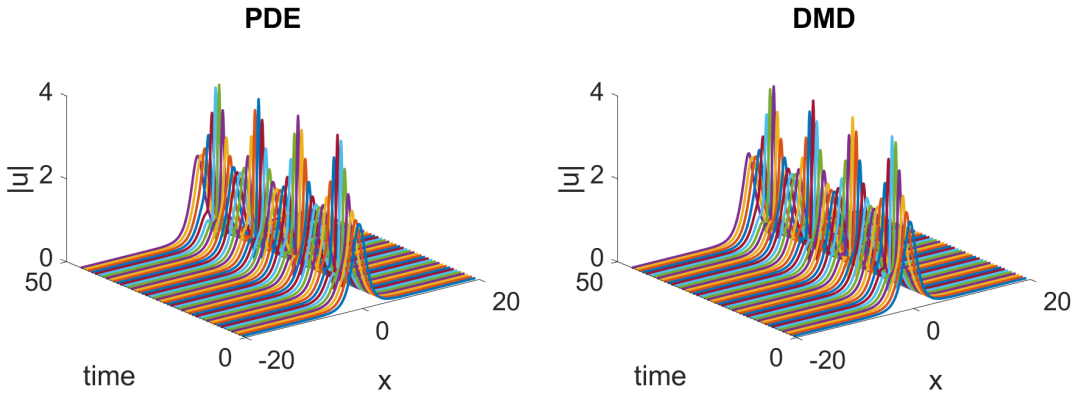

(e) (f)

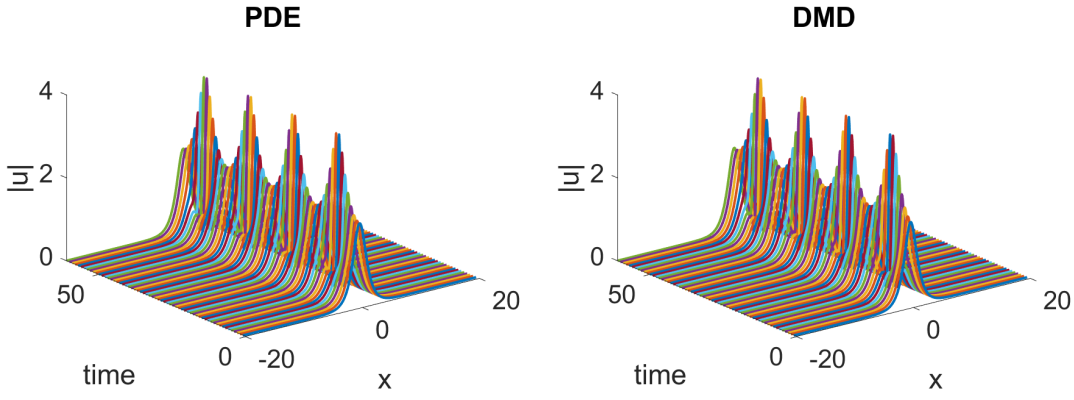

(g) (h)

Figure 9: The result of the simulation of the NLS equation over the interval $[0, 2\pi]$ at $N = 512$ spatial positions and at $M = 15, 30, 45, 60$ time points in a), c), e), and g) respectively. The predictions from DMD at each of these sampling levels in b), d) f) and h) respectively.

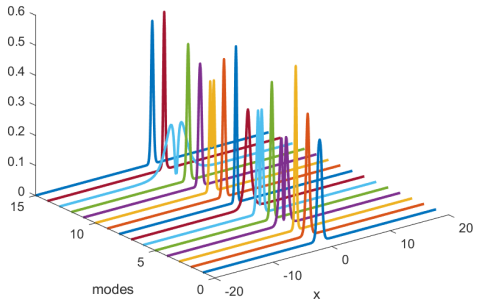

(a)

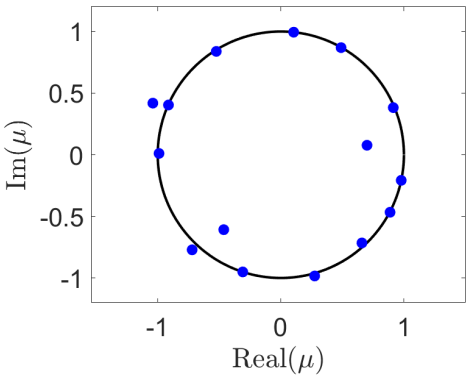

(b)

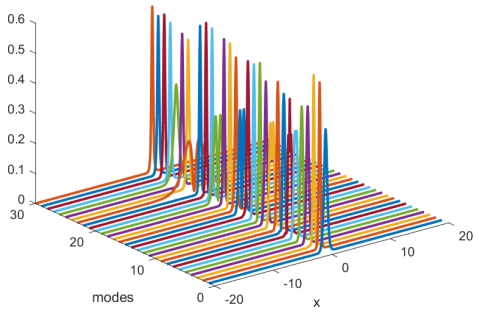

(c)

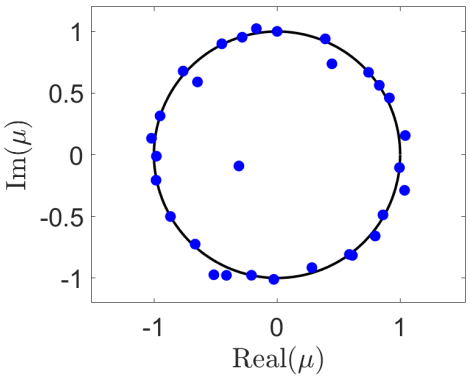

(d)

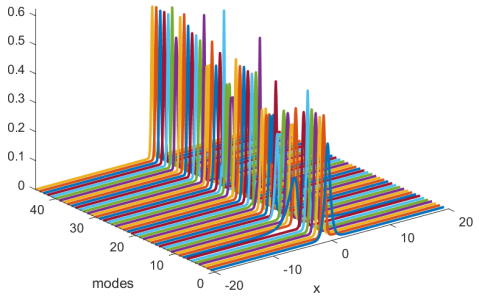

(e)

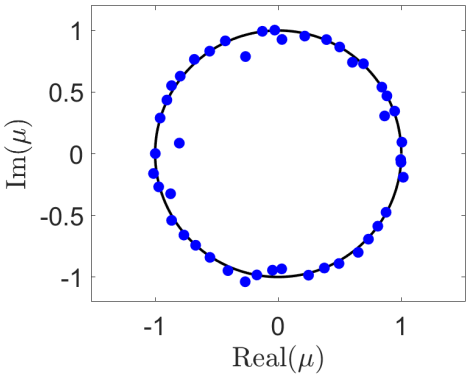

(f)

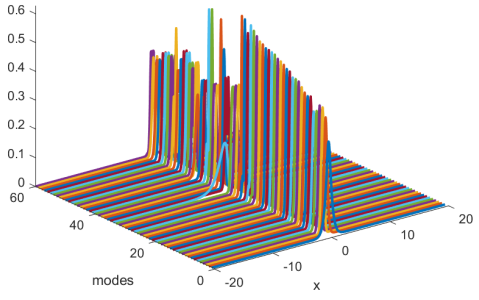

(g)

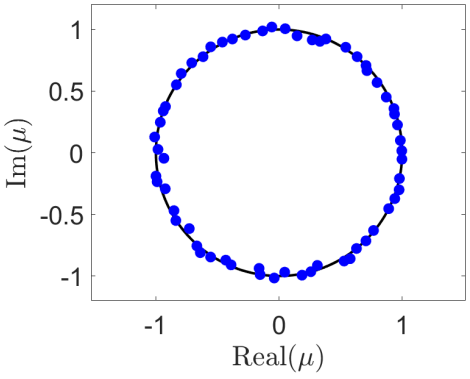

(h)

Figure 10: The DMD modes from data with $M = 15, 30, 45, 60$ time points in a), c), e), and g) respectively. The eigenvalue distribution at each of these sampling levels in b), d) f) and h) respectively.

5.2 Additive measurement noise

To understand how DMD performs with additive measurement noise we simulated the NLS equation over the time interval $[0, 2\pi]$ with $N = 512$ spatial points and $M = 60$ time-points. We then added noise sampled from a uniform distribution on the interval [0, 1]. The results from the simulation with the added noise is shown in Figure 11a and the DMD predictions are shown alongside in Figure 11b. The DMD predictions don't seem to match the simulated data as well as they did without the noise (see Figure 10g, h which was at the same sampling level). The DMD modes and eigenvalues from the data with this additive noise are shown in Figure 12. Comparing the eigenvalue distribution to that in Figure 10 we see that with the noise the eigenvalues lie further from the unit circle.

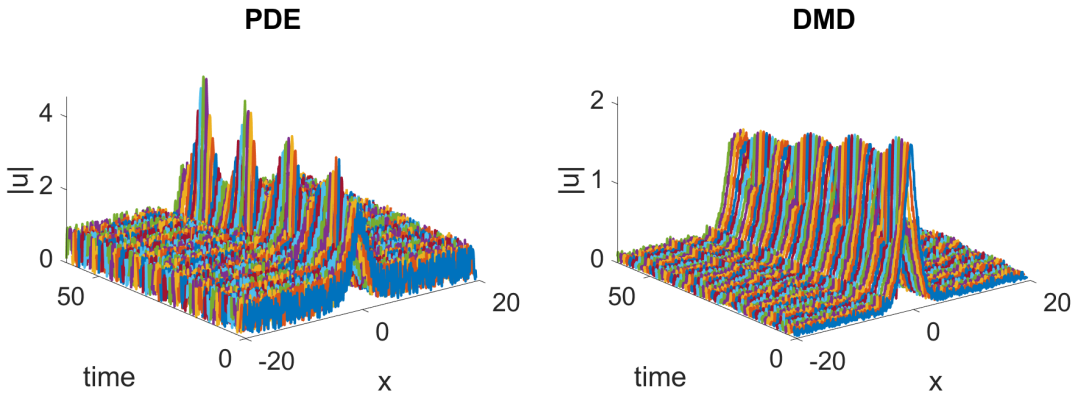

Figure 11: a) The result of the simulation of the NLS equation over the interval $[0, 2\pi]$ at $N = 512$ spatial positions, $M = 60$ time points and noise sampled from a uniform distribution on the interval [0, 1]. b) The predictions from DMD with this additive noise

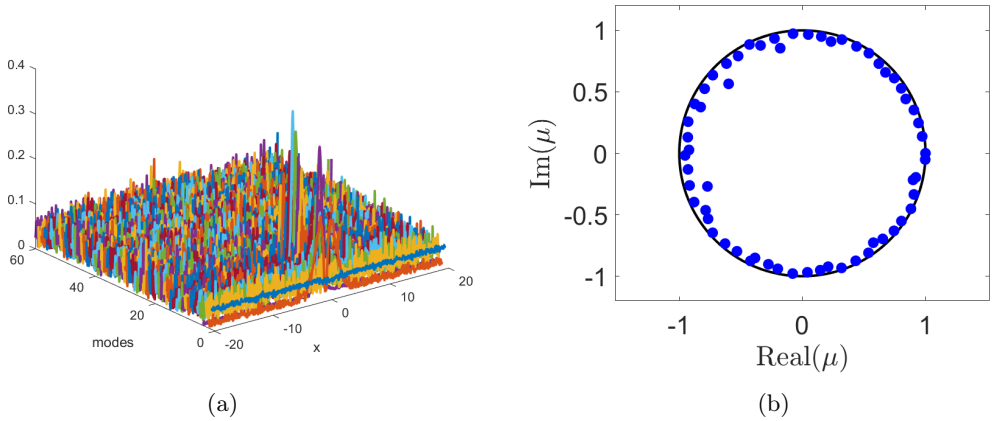

Figure 12: a) The DMD modes from data with $M = 60$ time points and noise sampled from a uniform distribution on the interval [0, 1]. b) The eigenvalue distribution with this additive noise

6 Conclusion

In our report, we explored DMDs ability to capture the dynamic modes of a system and then make predictions about the system at future times. We were able to describe the the eigenvalues of $\tilde{\mathbf{S}}$ and the dynamic modes uncovered by DMD for data simulated from the Nonlinear Schrodinger equation and data we were given of fluid flow past a cylinder. We also explored how DMD performance varies with reduced sampling in time and with additive noise. Both dense enough sampling in time and a low-enough noise level are necessary for optimal DMD performance.

References

[1] Schmid P. J. (2010). *Dynamic mode decomposition of numerical and experimental data.* Journal of Fluid Mechanics, 656, 5-28.

[2] Koopman B. O. (1931) *Hamiltonian systems and transformation in hilbert space.* Proceedings of the National Academy of Sciences, 17(5) 315-318.